Journal of Solid State Chemistry **154,** 584–590 (2000)
doi:10.1006/jssc.2000.8898, available online at http://www.idealibrary.com on IDEAL®

The Structure and Luminescent Properties of $TlZn(PO_3)_3$

A. El Abiad,* B. Es-Sakhi,† M. Mesnaoui,* M. Maazaz,* I. Belharouak, P. Gravereau, C. Parent, G. Wallez,‡ and G. Le Flem

*ICMCB, UPR, CNRS 9048, Avenue du DR Schweitzer 33608 Pessac, France; *Faculté des Sciences Semlalia-Marrakech, B.P. 2390, Marrakech, Morocco; †Département de Physique, Faculté des Sciences d'Agadir, Agadir, Morocco; and ‡Laboratoire de Cristallochimie du Solide, Université Pierre et Marie Curie, 4 Place Jussieu, 75252 Paris cédex 05, France*

Received April 13, 2000; in revised form July 7, 2000; accepted July 28, 2000; published online September 30, 2000

The crystal structure and the luminescent properties of $TlZn(PO_3)_3$ are studied with respect to Tl^+ stereochemistry. In this polyphosphate the Tl^+ ions are located in tunnels created by the zinc polyphosphate network $[Zn(PO_3)_3]$. Actually the thallium atoms are found in a disymmetric configuration and bond calculation allows the determination of the coordination number by oxygen: 6. Nevertheless a large Tl–O distance induces a low stereochemical activity of the $6s^2$ lone pair. The luminescent properties are analyzed in the context of Fukuda's model. Thermal variations of excitation and emission spectra can be explained by the small influence of the electron–lattice interaction in agreement with the thallium environment. © 2000 Academic Press

Key Words: **TlZn polyphosphate structure; Tl^+ stereoactivity; Tl^+ luminescence; lone pair effect.**

I. INTRODUCTION

Electronic ion polarizability of ns^2 ions such as Te^{4+}, Pb^{2+}, Bi^{3+}, Tl^+, etc., is attributed to the Lewis ns^2 free doublet which can generate structural and various specific physical properties. In the case of Tl^+ a review of the structural studies demonstrates the high anisotropic arrangement of anions around the Tl^+ ion. The localization of the lone pair was first determined by Verbaere *et al.* (1) by computing the electric field around the Tl(I) nucleus. Such electronic configuration induces high linear and nonlinear optical indices as a consequence of the hyperpolarizability of the thallium oxygen entities. For example, the rich thallium glasses of the TeO_2–Tl_2O system exhibit the highest optical nonlinear index reported presently for oxide glasses (2). Furthermore Tl_3PO_4 was investigated as an optical second harmonic generator (3).

In a parallel way, the luminescent properties Tl^+ ions in insulators have been the subject of several publications. In the studied materials, the Tl^+ ions are introduced as an impurity, e.g., in alkali halides (4) and in alkali–earth phosphates (5). The intense ultraviolet emission of β-$Ca_3(PO_4)_2$:Tl^+ was used in fluorescent lamps.

The interpretation of the luminescent spectra assumes the localization of the optical center in the cationic sites irrespective of the actual local structure at the Tl^+ site since the thallium concentration is very small. The Tl^+ emission bands labeled A_T (high energy) and A_X (low energy) were explained by a partial splitting of the emitting level by the Jahn–Teller effect(4).

The present paper describes in detail the structure and the preliminary investigation of the luminescent properties of $TlZn(PO_3)_3$. This thallium phosphate, previously reported by Averbuch-Pouchot (6), was selected as a model system in which the luminescent centers can be considered isolated since the thallium ions are 5.14 Å apart.

II. EXPERIMENTAL

(1) Chemical Preparation

The polyphosphate $TlZn(PO_3)_3$ was prepared by a solid state route from a mixture of ZnO, $(NH_4)_2HPO_4$ and Tl_2CO_3 in stoichiometric proportions according to the reaction

$$1/2Tl_2CO_3 + ZnO + 3(NH_4)_2HPO_4 \rightarrow TlZn(PO_3)_3 + 1/2\ CO_2 + 6NH_3 + 9/2H_2O.$$

The starting materials were ground together and heated at 200 and 300°C for 15 h to allow vapor phases to evolve. After a final grinding the mixture was heated at 500°C for 24 h. The obtained powder was white.

(2) Structural Investigation

The X-ray diffraction pattern was recorded at room temperature with a Philips X'PERT MPD(θ–θ) diffractometer using Cu$K\alpha$ radiation ($\lambda = 1.54060, 1.54442$ Å). The diffractometer was equipped with a graphite back monochromator, 0.02 rad. Sollers slits were introduced on incident and diffracted beams to decrease the line

0022-4596/00 $35.00

TABLE 1
X-Ray Diffraction Diagram of $TlZn(PO_3)_3$

h k l	d_{obs} (Å)	d_{cal} (Å)	I_{obs}	h k l	d_{obs} (Å)	d_{cal} (Å)	I_{obs}
0 0 2	6.49	6.49	4	1 5 2	2.046	2.046	1
0 2 0	5.94	5.94	2	2 3 2	2.040	2.041	2
0 2 1	5.40	5.40	17	0 2 6	2.033	2.034	2
1 0 0	5.12	5.12	16	2 0 4	2.011	2.010	2
1 1 1	4.42	4.42	6	1 3 5	2.000	1.999	1
0 2 2	4.38	4.38	5	1 0 6	1.994	1.993	1
1 0 2	4.02	4.02	6	2 1 4	1.982	1.982	3
1 1 2	3.81	3.81	28	0 6 0	1.979	1.980	1
1 2 1	3.72	3.72	100	1 1 6	1.966	1.966	2
0 2 3	3.50	3.50	35	0 6 1	1.958	1.958	3
1 2 2	3.33	3.33	18	0 4 5	1.955	1.955	0
0 0 4	3.245	3.25	10	2 4 0	1.939	1.939	2
1 1 3	3.184	3.18	4	2 3 3	1.926	1.925	5
1 3 0	3.134	3.13	6	2 2 4	1.904	1.904	2
1 3 1	3.046	3.05	6	1 2 6	1.890	1.889	2
0 4 0	2.969	2.970	2	2 4 2	1.858	1.858	5
1 2 3	2.889	2.888	11	1 6 0	1.848	1.847	7
0 2 4	2.848	2.848	3	1 6 1	1.828	1.828	3
1 0 4	2.741	2.741	41	1 5 4	1.797	1.796	4
0 4 2	2.702	2.701	30	2 3 4	1.793	1.792	1
2 0 0	2.560	2.559	7	0 2 7	1.770	1.770	1
1 3 3	2.538	2.537	9	0 4 6	1.749	1.749	6
1 4 1	2.521	2.520	2	2 2 5	1.744	1.743	3
2 1 0	2.502	2.502	4	1 1 7	1.726	1.726	0
0 4 3	2.449	2.449	1	1 6 3	1.700	1.699	3
1 4 2	2.389	2.389	14	0 6 4	1.691	1.691	4
2 0 2	2.382	2.381	2	2 5 2	1.683	1.682	4
0 2 5	2.378	2.379	19	3 1 1	1.674	1.675	2
2 1 2	2.335	2.335	9	2 3 5	1.655	1.656	1
2 2 1	2.312	2.313	1	3 1 2	1.6349	1.635	2
1 1 5	2.272	2.273	2	0 0 8	1.624	1.623	5
2 2 2	2.211	2.210	4	2 5 3	1.620	1.616	0
0 4 4	2.190	2.191	1	1 6 4	1.606	1.605	3
2 1 3	2.166	2.166	7	2 2 6	1.592	1.592	4
1 2 5	2.159	2.158	11	0 6 5	1.574	1.575	1
2 3 1	2.120	2.121	6	3 3 1	1.556	1.556	3
2 2 3	2.065	2.066	4	1 0 8	1.548	1.547	2

asymmetry at low θ: divergence slit of 1° and receiving slit of 0.05 mm. The holder surface was dusted with a 20-μm sieve. The rotation of the sample holder allowed a better statistical distribution of the crystallites. The data were recorded over the 12–110°(2θ) angular range with a 0.02° step and a fixed counting time of 30 s.

(3) Optical Measurements

Excitation and emission spectra were recorded between 4 and 300 K using a SPEX FL212 fluorometer equipped with a SMC liquid helium cryostat. The continuous emission of a 450-W xenon lamp was used as the excitation source. The emission and excitation wavelengths were dispersed by two monochromators in a Czerny-Turner configuration. The emission was detected with a Hamamatsu R928 photomultiplier.

III. STRUCTURE OF $TlZn(PO_3)_3$

(1) Cell Parameters and Symmetry

The X-ray diffraction pattern was indexed in orthorhombic symmetry with the following parameters: $a = 5.1192(5)$ Å, $b = 11.8822(5)$ Å, and $c = 12.9827(5)$ Å. These parameters are close to those previously reported: $a = 5.125$ Å, $b = 11.900$ Å, and $c = 13.010$ Å (6). The experimental density 4.19 is close to the value 4.26 deduced from the X-ray data with $4TlZn(PO_3)_3$ formula per unit cell. In the indexation of the X-ray diffraction diagram (Table 1), the observed reflection conditions (0, k, l):$k = 2n$ and (h, 0, l):$l = 2n$ are consistent with two space groups $Pbc2_1$ and $Pbcm$. All these structural data are close to those of the orthorhombic form of $NH_4Co(PO_3)_3$, the structure of which was solved assuming the $Pbcm$ S.G (7).

(2) Structure Determination

The structure determination was developed with the following steps:

(i) The profile of the diffraction lines was calculated, independently of any structural model, to test the $Pbcm$ S.G. using the "profile matching" option of the FULLPROF program (8). The final characteristic indices were, respectively, $cR_{wp} = 0.15$ and $\chi^2 = 1.8$.

(ii) The initial atomic coordinates were those proposed for $NH_4Co(PO_3)_3$. The agreement factor—$cR_{wp} = 0.80$—was very high. This divergence was attributed to a wrong position of the thallium atom.

(iii) An investigation of the Tl atomic position was undertaken by trials of the Patterson function deconvolution (program SHELXS-86) with 72 structure factors of the first best-resolved reflections (no neighbor reflections at less than one FWHM apart in the angular range $\theta < 40°$). This procedure led to a hypothetical location of the Tl atoms strongly different from the "NH_4" site used in (ii).

(iv) Then the positional parameters of the ammonium cobalt polyphosphate were used for P, O, and Zn (in the Co site) to build a new structural model before a final Rietveld refinement process (program FULLPROF (8)). Such calculations lead to satisfactory profile factors ($cR_P = 0.129$, $cR_{wp} = 0.15$) and crystal structure model indicators $R_B = 0.051$ and $R_F = 0.050$. A tentative refinement in the context of the acentric S.G. $Pbc2_1$ does not improve significantly the structural model. The conditions for the data collection and the parameters of the Rietveld refinement are listed in Table 2.

TABLE 2
Conditions for Data Collection and Details of Reitveld Refinement

Wavelength (Å)	$\lambda K_{\alpha 1} = 1.54060$ $\lambda K_{\alpha 2} = 1.54443\,\mathrm{I}K_{\alpha 1}/\mathrm{I}K_{\alpha 2} = 0.47$
Step scan increment (°2θ)	0.02
2θ range (°)	12–110
Program	FULLPROF (8)
$TlZn(PO_3)_3$ as unique phase	
Pseudo-Voigt function $PV = \eta L + (1-\eta)G$	$\eta = 0.54(2)$
Cagliotti law parameters (9)	$U = 0.051(9)$, $V = 0.013(7)$, $W = 0.002(1)$
Preferred orientation parameter ([0 0 1]*); correction using the function of March (10)	0.967(4)
Space group	*Pbcm*
a (Å)	5.1192(5)
b (Å)	11.8822(9)
c (Å)	12.9827(9)
d_X	4.26
d_{exp}	4.19
Z	4
No. of reflections	1060
No. of refined parameters	42
$R_{p\,\text{including the background}}$	0.078
$R_{wp\,\text{including the background}}$	0.102
$cR_{p\,\text{excluding the background}}$	0.129
$cR_{wp\,\text{excluding the background}}$	0.150
Discrepancy factors	$R_B = 0.051$, $R_F = 0.050$, $\chi^2 = 2.25$

Figure 1 presents a comparison of the experimental and calculated X-ray diffraction data. The resulting atomic coordinates and their e.s.d. values are given in Table 3.

Table 4 gives selected bond lengths (Å) and angles (°) for $TlZn(PO_3)_3$. These results are satisfactory insofar as the next neighbors oxygen atoms surrounding the thallium atoms are located at distances larger than 3.68 Å.

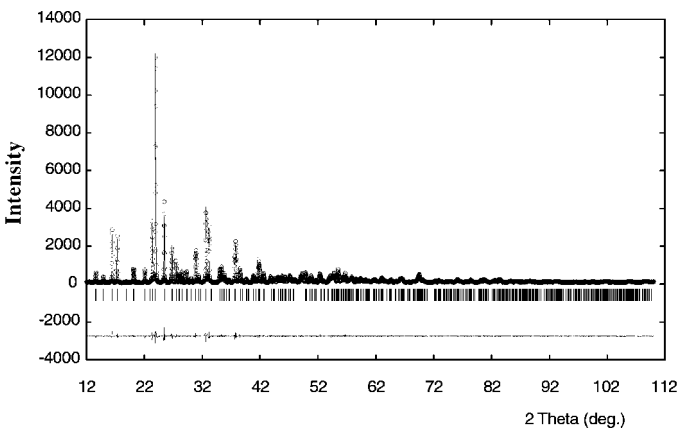

FIG. 1. Comparison between the experimental (ooo) and calculated (—) X-ray diffraction patterns.

TABLE 3
Atomic Coordinates and Thermal Parameters of $TlZn(PO_3)_3$

Element	Wyckoff site	*x*	*y*	*z*	B_{iso} (Å^2)
Tl	4(d)	0.076(1)	0.145(1)	$\frac{1}{4}$	1.78(2)
Zn	4(a)	0	0	0	3.27(1)
P(1)	4(c)	0.751(3)	$\frac{1}{4}$	0	0.87(2)
P(2)	8(e)	0.489(2)	0.415(1)	0.135(1)	0.87(2)
O(1)	8(e)	0.547(4)	0.299(2)	0.084(1)	0.79(3)
O(2)	8(e)	0.901(4)	0.158(2)	0.051(1)	0.79(3)
O(3)	8(e)	0.204(4)	0.437(2)	0.126(6)	0.79(3)
O(4)	8(e)	0.672(4)	0.498(2)	0.097(1)	0.79(3)
O(5)	4(d)	0.551(5)	0.382(2)	$\frac{1}{4}$	0.79(3)

Actually the thallium atom is located in a wide cavity limited by four metaphosphate chains and two ZnO_6 octahedra forming a 15-oxygen polyhedron. The Tl–O distances range from about 2.81 to 3.90 Å, corresponding to bond strengths fading from 0.175 to 0.025 valence units (13), but the cumulated value (0.997 v.u.) shows that even the furthest ones must be taken into account, although very distant. Nevertheless a reduced coordination polyhedron can be defined by the six oxygen atoms of two ZnO_6 octahedra faces that share 91% of the thallium valence.

TABLE 4
Selected Bond Lengths (Å) and Bond Valence Parameters for $TlZn(PO_3)_3$

Structural entities	Distances (Å)	Bonds valence parameters
	ZnO_6 octahedron	
Zn–O(2) × 2	2.053(2)	2 × 0.389
Zn–O(3) × 2	2.084(2)	2 × 0.358
Zn–O(4) × 2	2.097(2)	2 × 0.346
		Σs = 2.18 Valence: 2
	PO_4 tetrahedra	
P(1)–O(1) × 2	1.619(2)	2 × 0.99
P(1)–O(2) × 2	1.493(2)	2 × 1.40
		Σs = 4.8 Valence: 5
P(2)–O(1)	1.561(2)	1.16
P(2)–O(3)	1.486(2)	1.42
P(2)–O(4)	1.448(2)	1.58
P(2)–O(5)	1.572(1)	1.13
		Σs = 5.29 Valence: 5
	Tl environment	
Tl–O(2) × 2	2.736 (2)	2 × 0.25
Tl–O(4) × 2	2.943(2)	2 × 0.346
Tl–O(3) × 2	3.278(2)	2 × 0.06
	Other Tl–O bonds > 3.68 Å	Σs = 0.91 Valence: 1

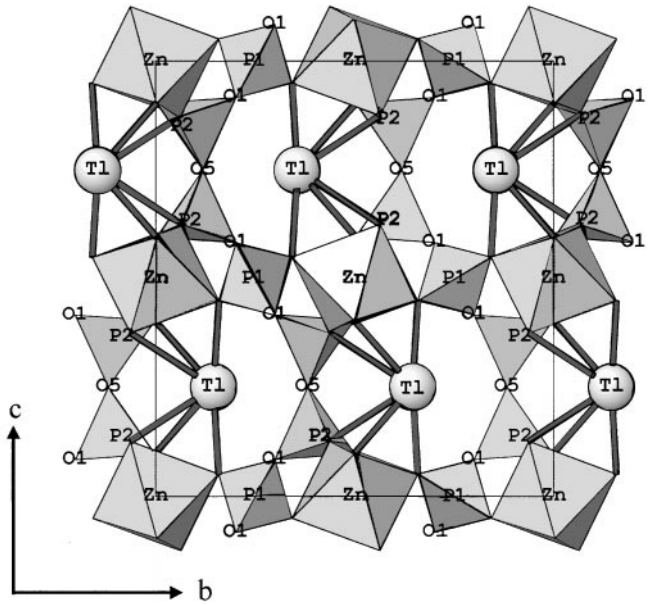

FIG. 2. Structure of $TlZn(PO_3)_3$: view along the *a* axis.

(3) Thallium(I) Environment

In such a wide cavity, even large cations such as thallium or heavy alkalii (K^+, Rb^+, Cs^+) are generally off-center and show widely scattered bond lengths. In the case of thallium, it was necessary to estimate the stereochemical effect of the cation, i.e., the ability for the $6s^2$ lone pair to fill the space close to the thallium core. In this context, it is commonly known that *p*-block cations with $ns^2\ np^0$ electronic configuration are likely to show a partial hybridization of the s^2 pair, leading to the formation of a local dipole that may strongly affect the cation–anion distances.

A simple method was suggested by Verbaere *et al.* (1), who considered the Tl^+ cation as a Tl^{3+}–E^{2-} dipole, the momentum of which could be given by the local electrostatic field *E*. Assuming that the high polarizability $\alpha = 7.28\ Å^3$ of the cation (14) is due mainly to the presence of the bulky and screened lone pair, the corresponding equation can be written as

$$\alpha \cdot E = 2e \cdot \text{Tl–}E,$$

where $2e$ is the lone pair charge.

The program HYBRIDE (15) was run by loops until reaching the self-consistent position of the lone pair, assuming various ionic charge models:

— the formal one, that is the oxidation states of the ions;
— the empirical Pauling's model (16), based upon the electronegativity differences that gave Tl, + 0.65; Zn, + 1.13; and P, + 2.0; and
— a more recent model of bond ionicity (17), giving Tl, + 0.94; Zn, + 1.64; and P, + 1.90.

In the two latter cases, a common balancing charge was given to all oxygen anions.

Although slightly different, the three models gave similar results, with the most stable position for the lone pair on the opposite of the six closest oxygen atoms, in the mirror plane, at about 0.2 Å from the nucleus (Fig. 3). This distance is short and accounts for a low stereochemical activity. For instance, an active lone pair is generally found at 0.4–0.7 Å as in Tl_2O, TlOH, Tl_4O_3 (1), and some other compounds (Table 5).

This result can be correlated to the structural features of $TlZn(PO_3)_3$ insofar as it indicates that the off-centered position of the Tl^+ cation is not due to the lone pair presence. Indeed, a strong stereochemical activity is observed in structures where the lone pair bearers are highly concentrated and compelled to occupy sites with few anion neighbors. In this case, the s^2 hybridization allows the splitting of the M^{n+} cation in a $M^{(n+2)+}$ core and a "free" – 2 charge. So, the small and positive-charged core can take place very close to some of the oxygen neighbors and the lone pair can be found near the center of the global coordination polyhedron. It is noteworthy that in such compounds, the shortest M^{n+}–O^{2-} distances are nearly equal to common $M^{(n+2)+}$–O^{2-} ones, as can be seen in Table 5, i.e., for Tl_2O, Tl_2TiO_3, and Tl_2TeO_3, assuming a distance Tl^{3+}–O^{2-} = 2.36 Å instead of the mean Tl^+–O^{2-} = 2.98 Å (11). In $TlZn(PO_3)_3$, the shortest Tl–O bonds are clearly longer and also account for a low hybridization rate.

Moreover in the isomorphic phosphate $NH_4Co(PO_3)_3$ (7), the NH_4–O distances are also widely scattered, proving that the thallium behavior in the title compound is not due to the lone pair.

Such a low "lone pair" activity which seems incompatible with the strong dissymmetric environment of the thallium by the closest oxygen atoms must be discussed in the context of the main characteristics of the whole structure.

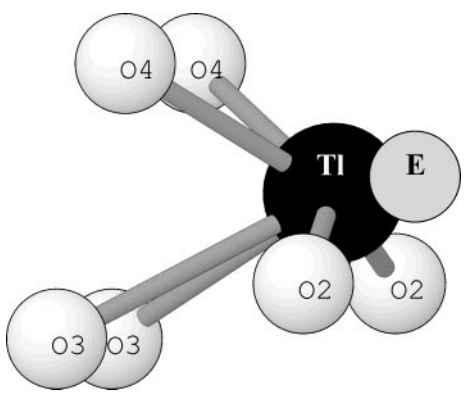

FIG. 3. Thallium environment and localization of the lone pair.

TABLE 5
Minimum Tl–O Distances in Several Oxides and Corresponding Calculated Tl–Lone Pair Distances According Ref. (1)

Compound	Shorter Tl–O distances (Å)	Tl–E (Å)	Ref.
Tl_2CO_3	2.68–2.67	0.38–0.31	18
$Tl_6Si_2O_7$	2.41–2.38	0.52– 0.39	19
Tl_2TiO_3	2.48–2.41	0.39–0.47	20
Tl_2SnO_3	2.49–2.53	0.47– 0.49	21
Tl_3PO_4	2.53	0.42	3
$TlSrVO_4$	2.56		22
$TlBaVO_4$	2.69		22
$TlSbO_3$	2.54		23
Tl_2O	2.52–2.51	0.52–0.52	24
Tl_2TeO_3	2.44		25
$Tl_2Te_3O_7$	2.47		26

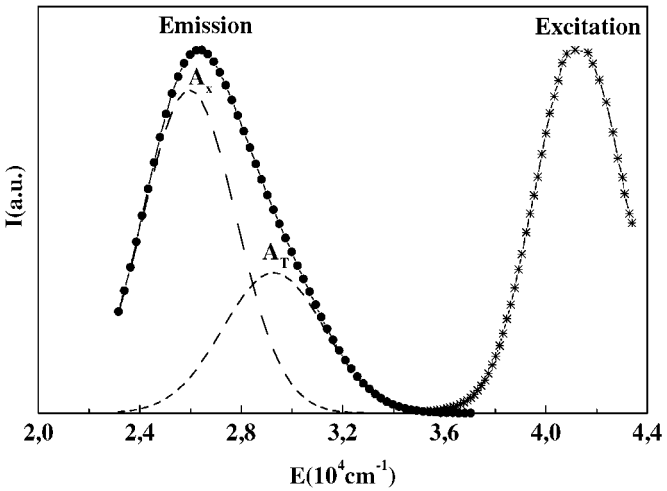

FIG. 4. Excitation ($\lambda_{em.} = 380$ nm) and emission ($\lambda_{exc.} = 250$ nm) spectra of $TlZn(PO_3)_3$ at $T = 6$ K.

The sublattice $[Zn(PO_3)_3]$ is a covalent network made up of eight-member rings forming channels along the $\vec{b}$ axis. These channels contain only one crystallographically independent Tl cation. The three shorter Tl–O distances involve the O(2), O(3), and O(4) oxygen which are also located at the common corner of the $[PO_4]$ tetrahedra and $[ZnO_6]$ octahedra. This covalent framework induces rather ionic antagonist Tl–O bonds, which is consistent with the rather large Tl–O distances. Similar argument can be mentioned to explain the Tl–O distances in $TlZnXO_4$ (X = P, As)(27). In these compounds, the thallium is located in the channels of a covalent framework formed by alternating $[XO_4]$ and $[ZnO_4]$ tetrahedra. The Tl–O distances are larger than 2.743 Å in the phosphate and larger than 2.720 Å in the arsenate. For comparison, in most thallium oxides the minimum Tl–O distances are rather smaller (Table 5).

In this context the low stereochemical activity of the Tl(I) lone pair in the investigated phosphate can be explained by the Tl environment with oxygens at distances larger than 2.7 Å. Such a structural configuration tends to lower the electrostatic repulsion between the $6s^2$ cloud and the first neighbor oxygens.

IV. LUMINESCENT PROPERTIES OF $TlZn(PO_3)_3$

(1) Luminescence Spectra

The emission and excitation spectra have been investigated between 6 and 300 K.

At 6 K the emission spectrum recorded under a 250-nm excitation exhibits a broad band that can be decomposed into two bands peaking, respectively, at 30,770 cm^{-1} (325 nm), labeled A_T, and at 25,500 cm^{-1} (380 nm), labeled A_X, (Fig. 4). The excitation spectrum of the A_X emission is a broad band with a maximum at about 41,000 cm^{-1} (243 nm) whereas the excitation spectrum of the A_T emission is detected as an intense band with an apparent maximum at 230 nm. Actually such a maximum can result from the experimental conditions, this energy range corresponding to the limit of the fluorescence detection and the true maximum is probably located at higher energy. An additional band with low intensity can be detected at about 250 nm (Fig. 5).

By increasing the temperature:

—Under a 250-nm excitation, the A_X emission intensity decreases whereas the A_T emission intensity increases. This last emission is only observed at room temperature (Fig. 6).

—Under a 230-nm excitation, only the A_T emission is observed with approximately the same intensity and a slight blue shift of the band maximum (Fig. 7).

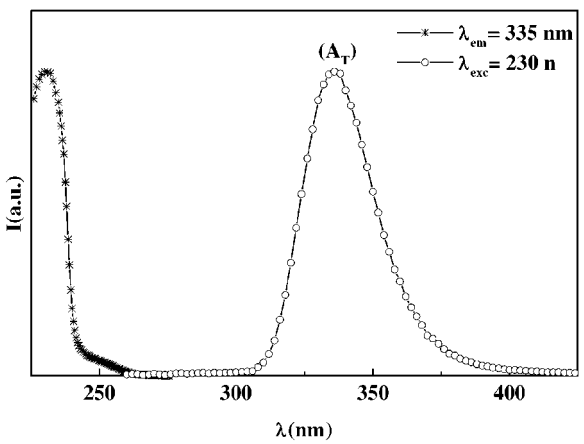

FIG. 5. Excitation ($\lambda_{em.} = 335$ nm) and emission ($\lambda_{exc.} = 230$ nm) spectra of $TlZn(PO_3)_3$ at $T = 6$ K.

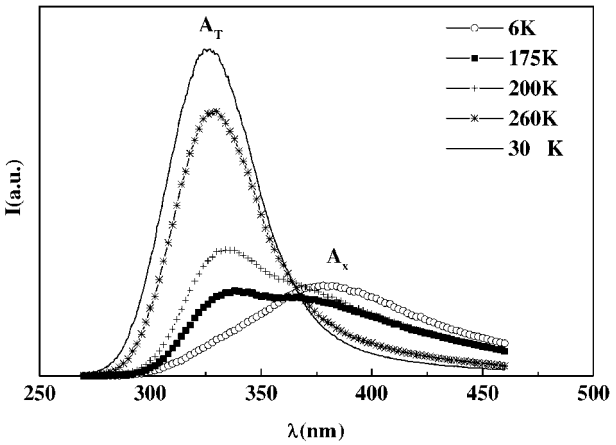

FIG. 6. Thermal variation of the intensity maxima of the A_T and A_X emission bands under a 250-nm excitation.

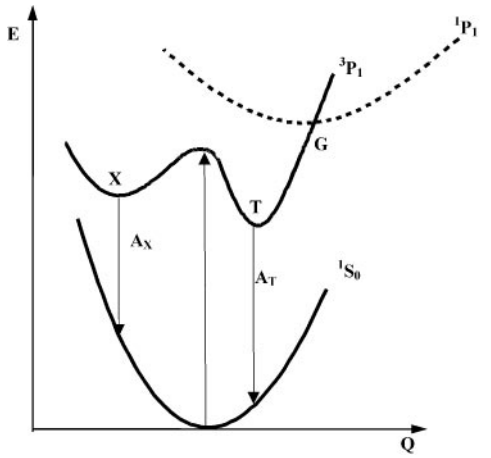

FIG. 8. Hypothetical configuration curves of the thallium $^1S_0$, $^3P_1$, and $^1P_1$ levels. The T and X minima stand for the respective origins of the A_T and A_X emissions.

(2) Discussion

The Tl^+ luminescence involves $6s^2 \Leftrightarrow 6s6p$ transitions. The $6s^2$ electronic configuration is responsible for the $^1S_0$ ground state, whereas the first $6s6p$ excited states are successively $^3P_0$, $^3P_1$, $^3P_2$, and $^1P_1$ with increasing energy (28). The analysis of the crystal structure allows us to neglect the effect of the crystal field in the first approximation. Moreover the complex environment of Tl^+ makes it difficult to deduce the kind of distortion produced by the respective contribution of the spin–orbit interaction and the electron–lattice interaction. Both the large Tl–O distances and the small stereochemical activity of the $6s^2$ lone pair become clear in that the former parameter is of suitable value as compared to the latter. In this situation the model of Fukuda (4) predicts two kinds of minima such as T and X in the potential energy surface of the relaxed $^3P_1$ excited state.

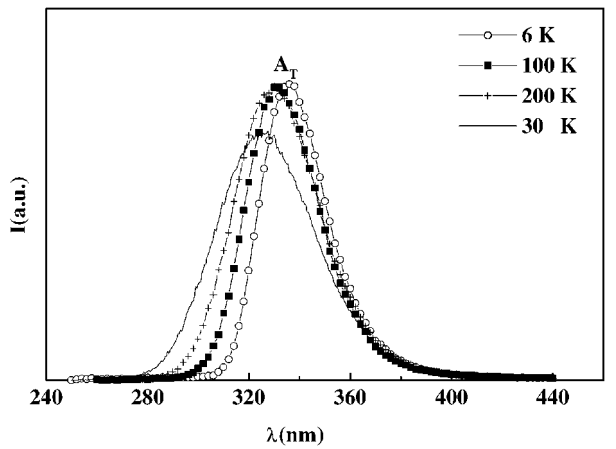

FIG. 7. Thermal variation of the A_T emission of $TlZn(PO_3)_3$ under a 230-nm excitation.

In Tl-doped alkali halides and related compounds, the high-energy emission band A_T is first observed at low temperature with a small percentage of the A_X emission. Above various temperatures, depending on the considered materials, the A_T emission decreases whereas the A_X emission increases (see Fig. 1 of Ref. (4)). Such behavior is exactly the opposite thermal evolution of the A_X and A_T emission intensities of the phosphate. Therefore at the present stage of the investigation the following qualitative model is considered to account for the experimental data. Hypothetical configuration curves are schematically shown in Fig. 8.

The excitation bands peaking at $\lambda = 250$ and 235 nm are respectively ascribed to the $^1S_0 \rightarrow {}^3P_1$ and $^1S_0 \rightarrow {}^1P_1$ transitions. At low temperature a 250-nm excitation populates preferentially X but also T minima whereas a 235-nm excitation populates only T through the G crossing point connecting the $^1P_1$ and the $^3P_1$ curves. In the former case as the temperature is raised, T is populated at the expense of X. In the second case whatever the temperature, only T is populated, which involves for the $^3P_1$ curve a T minimum energy below the X minimum energy.

V. CONCLUSIONS

The crystal structure of the polyphosphate $TlZn(PO_3)_3$ can be described as made up of infinite phosphate chains connected by almost regular ZnO_6 octahedra. The Tl^+ ions are located in the tunnels created by the zinc polyphosphate network $[Zn(PO_3)_3]$ in a strongly irregular site typical of lone pair ions. They are coordinated by six nearest neighbor oxygen atoms in agreement with bond valence calculation. The corresponding large Tl–O distances lower the electrostatic repulsion between the $6s^2$ cloud and the surrounding oxygens, which explains the low stereoactivity of the $6s^2$–Tl^+ lone pair.

The luminescent properties are analyzed in the context of Fukuda's model. However the thallium site of the phosphate is strongly different from the assumed thallium site in alkali halides, which makes it difficult to give a theoretical framework explaining quantitatively the experimental results. The characteristic features of the excitation and emission spectra can be qualitatively described by a system of configuration curves, assuming a small effect of the electron–lattice interaction in agreement with the characteristics of the thallium environment.

REFERENCES

1. A. Verbaere, R. Marchand, and M. Tournoux, *J. Solid State Chem.* **23,** 383 (1978).
2. B. Jeansannetas, S. Blanchandin, P. Thomas, P. Marchet, J. C. Champarnaud-Mesjard, T. Merle-Mesjan, B. Frit, V. Nazabal, E. Fargin, G. Le Flem, M. O. Martin, B. Bousquet, L. Canoini, S. Le Boiteux, P. Segonds, and L. Sarger, *J. Solid State Chem.* **146,** 329 (1999).
3. A. Zalkin, D. H. Templeton, D. Eimerland, and S. P. Velsko, *Acta Crystallogr. C* **42,** 1686 (1986).
4. A. Fukuda, *Phys. Rev. B* **1**(10), 4161 (1970).
5. A. C. Van der Steen and Th. J. A. Aalders, *Phys. Status Solidi B* **103,** 803 (1981).
6. M. T. Averbuch-Pouchot, *Bull. Soc. Fr. Mineral. Cristallogr.* **95,** 558 (1972).
7. Tranqui Duc, J. C. Grenier, A. Durif, and J. C. Guitel, *Bull. Soc. Fr. Mineral. Cristallogr.* **90,** 252(1967).
8. J. Rodriguez-Carvajal, i*n* "Collected Abstracts of Powder Diffraction Meeting, Toulouse, France, 1990," p. 127.
9. G. Cagliotti, A. Paoletti, and F. P. Ricci, *Nucl. Instrum.* **3,** 223 (1958).
10. A. March, *Z. Kristallogr.* **81,** 285 (1932).
11. R. D. Shannon, *Acta Crystallogr. A* **32,** 751 (1976).
12. I. D. Brown and D. Altermatt, *Acta Crystallogr. B* **41,** 244 (1985).
13. I. D. Brown and K. K. Wu, *Acta Crystrallogr. B* **32**, 1957 (1976).
14. R. D. Shannon, *J. Appl. Phys.* **73,** 348 (1993).
15. G. Wallez, "HYBRIDE: A program for the research of lone pairs in crystalline solids," Université Pierre et Marie Curie, France, 1999.
16. L. Pauling, "The Nature of the Chemical Bond," Cornell Univ. Press, New York, 1939.
17. Y. Y. Guo, C. K. Kuo, and P. S. Nicholson, *Solid State Ionics* **123,** 225 (1999).
18. R. Marchand, Y. Piffard, and M. Tournoux, *Can. J. Chem.* **53**(16), 2454 (1975).
19. Y. Piffard, R. Marchand, and M. Tournoux, *Rev. Chim. Miner.* **12,** 210 (1975).
20. A. Verbaere, M. Dion, and M. Tournoux, *J. Solid State Chem.* **11,** 60 (1974).
21. A. Verbaere, M. Dion, and M. Tournoux, *J. Solid State Chem.* **11,** 184 (1974).
22. J. Boje and Hk. Müller-Buschbaum, *Z. Anorg. Allg. Chem.* **611,** 137 (1992).
23. M. Bouchama and M. Tournoux, *Rev. Chim. Miner.* **12,** 80 (1975).
24. H. Sabrowsky, *Z. Anorg. Allg. Chem.* **381,** 266 (1971).
25. B. Frit and D. Mercurio, *Rev. Chim. Miner.* **17,** 192 (1980).
26. B. Jeansannetas, P. Thomas, J. C. Champarnaud-Mesjard, and B. Frit, *Mater. Res. Bull.* **32**(1), 51 (1997).
27. M. Andratschke, K. J. Range, C. Weigl, U. Scheiβl, and F. Rau, *Z. Naturforsch.* **49b,** 1282 (1994).
28. D. Curie (Ed.), "Champ Cristallin et Luminescence." Gauthier–Villars, Paris, 1968.